Biocatalysis, Protein Engineering and Nanobiotechnology **Biotechnology and Bioengineering**
DOI 10.1002/bit.25996

Designed Protein Aggregates Entrapping Carbon Nanotubes for Bioelectrochemical Oxygen Reduction†

Kristen E Garcia,[1,‡] Sofia Babanova,[2,‡] William Scheffler,[3] Mansij Hans,[1] David Baker,[3] Plamen Atanassov,[2] Scott Banta[1,*]

[1]Department of Chemical Engineering, Columbia University, 500 West 120th Street, New York, NY 10027
[2]Department of Chemical and Biological Engineering, University of New Mexico, Albuquerque, NM 087131
[3]Department of Biochemistry, University of Washington, Seattle, WA 98195

Running Title: Designed protein aggregates for oxygen reduction

‡K. E. Garcia and S. Babanova contributed equally to the work

*To whom correspondence should be addressed:
Email: sbanta@columbia.edu
Telephone: (212) 854-7531
Fax: (212) 854-3054

Additional Supporting Information may be found in the online version of this article.

Received October 31, 2015; Revision Received April 6, 2016; Accepted April 11, 2016

Abstract:

The engineering of robust protein/nanomaterial interfaces is critical in the development of bioelectrocatalytic systems. We have used computational protein design to identify two amino acid mutations in the small laccase protein (SLAC) from *Streptomyces coelicolor* to introduce new inter-protein disulfide bonds. The new dimeric interface introduced by these disulfide bonds in combination with the natural trimeric structure drive the self-assembly of SLAC into functional aggregates. The mutations had a minimal effect on kinetic parameters, and the enzymatic assemblies exhibited an increased resistance to irreversible thermal denaturation. The SLAC assemblies were combined with single-walled carbon nanotubes (SWNTs), and explored for use in oxygen reduction electrodes. The incorporation of SWNTs into the SLAC aggregates enabled operation an elevated temperature and reduced the reaction overpotential. A current density of 1.1 mA/cm^2 at 0 V vs. Ag/AgCl was achieved in an air-breathing cathode system.

Key words: protein design, self-assembly, laccase, oxygen reduction reaction, protein/nanomaterial interface

Introduction

A grand challenge in the development of efficient bioelectrocatalytic systems is the optimization of transport and reaction kinetics within robust electrode surface modifications. The incorporation of enzymes into these systems presents unique challenges including operational stability, poor compatibility with entrapping polymer matrices, and optimizing spatial arrangements with mediating or relay systems (Kim et al., 2006; Minteer et al., 2007). A variety of materials engineering approaches have been developed to better enable the incorporation of native enzymes into electrode systems (Addo et al., 2010; Lau et al., 2012; Lim et al., 2007), and a few protein engineering approaches have been used to improve the protein/nanomaterial interface (Holland et al., 2011; Szilvay et al., 2011; Wong and Schwaneberg, 2003).

Computational protein design has been successfully used to engineer almost every feature of proteins, including binding, stability and catalysis (Jiang et al., 2008; King et al., 2012; King et al., 2014; Korkegian et al., 2005; Padilla et al., 2001; Usui et al., 2009). A recent trend is the use of protein design principles to create non-natural assemblies of protein structures to generate long-range order in self-assembling systems (Padilla et al., 2001; Usui et al., 2009). These unique protein structures show great promise for the development and improvement of bio/nano interfacial systems as these arrangements can lead to improved stability and optimized spatial orientations.

Multi-copper oxidase enzymes directly reduce oxygen and have been extensively explored for use in enzymatic bio-cathodes to be used in biological fuel cells (BFCs), bio-batteries and self-powered bio-sensors (Babanova et al., 2014; Lau et al., 2012; Tsujimura et al., 2007). BFCs are devices that utilize biocatalysts for energy transformation (Barton et al., 2004; Cooney et al., 2008; Davila et al., 2008; Logan et al., 2006; Luckarift et al., 2014). Since the

chemical energy stored in ubiquitous fuels available in the environment is transformed into electricity in BFCs, the practical application of these systems is often associated with energy harvesting. BFCs using enzymes as catalytic units are predominantly associated with the design of small devices, generating relatively high power (Luckarift et al., 2014). The critical drawback of enzymatic BFCs is their operational lifetime, which can be limited by the environmental stability of immobilized enzymes.

The fungal laccases have been well-studied for the development of bio-cathodes due to their high activity and redox potential, but the engineering of these proteins is more challenging as they generally do not express well in prokaryotic hosts (Glykys et al., 2011). Bacterial laccases, such as the small laccase (SLAC) from *Streptomyces coelicolor* can have lower redox potentials but are more active at neutral pH and are more amenable to protein engineering strategies (Machczynski et al., 2004). Previously, the trimeric SLAC enzyme has been combined with single-walled carbon nanotubes (SWNTs) and also engineered to form self-assembling protein hydrogels with osmium redox centers, demonstrating its utility as a biocathode modification (Gallaway et al., 2008; Szilvay et al., 2011; Wheeldon and Gallaway, 2008). Here we use computational design to identify mutations for the introduction of new inter-protein disulfide bonds that would enable the SLAC enzyme to self-assemble into stable, functional crystalline-like assemblies.

Materials and Methods

Materials

Oligonucleotides were purchased from Integrated DNA Technologies (Coralville, IA). All cloning enzymes and *E. coli* BL21 (DE3) competent cells were from New England Biolabs (Ipswich, MA). Isopropyl β-D-1-thiogalactopyranoside (IPTG) was from Gold Biotechnology (St. Louis, MO). HALT

protease inhibitor, Pierce Coomassie (Bradford) Protein Assay Kit, precast NuPAGE SDS-PAGE gels, NuPAGE SDS MES running buffer and Novex Sharp Pre-stained Protein Standard were from Thermo Fisher Scientific (Waltham, MA). HisTrap FF columns and the ÄKTA FPLC system were purchased from GE Healthcare (Piscataway, NJ). Uranyl acetate was purchased from Polysciences Inc. (Warrington, PA). Carbon black Vulcan X72 was purchased from Cabot Corporation (Boston, MA), Carbon coated 400 mush Cu/Rh grids were purchased from Ted Pella Inc (Redding, CA). All other chemicals were purchased from Sigma-Aldrich (St. Louis, MO) at the highest purity unless otherwise specified.

Construction, expression and purification of enzymes

The pSLAC-His vector encodes for the SLAC enzyme from *Streptomyces coelicolor* with a C-terminal His_6-tag (Szilvay et al., 2011). The Gly70 and Ala189 amino acids were mutated to cysteine by site-directed mutagenesis generating pSLAC-DC-His **(**Table S1). The vector pSLAC-DC-His was transformed into *E. coli* BL21(DE3) cells for SLAC-DC-His protein expression.

Cells were grown in 2xYT media at 37°C. At OD_{600} ~1.5, protein expression was induced by the addition of 0.4 mM IPTG, and the cells were grown an additional 20 hours at 25°C. Cells were collected by centrifugation and stored at -20°C. Frozen cell pellets corresponding to 1 L of culture were thawed on ice for 30 minutes and the suspended in 50 mL of Buffer A (20 mM sodium phosphate buffer, 40 mM imidazole, 50 mM NaCl at 7.3 mM) with HALT EDTA-free protease inhibitor. Cells were sonicated for 6 minutes using a microtip probe, and lysates were centrifuged for 30 minutes at 15,000 x *g*. Lysates were applied to a HisTrap FF column equilibrated with Buffer A, and bound proteins were eluted with a linear gradient of 0 to 100% Buffer B (20 mM sodium phosphate buffer, 500 mM Imidazole, 500 mM NaCl at 7.3 mM) using an ÄKTA FPLC system. Fractions containing SLAC-His or SLAC-DC-His shown by SDS PAGE with bands at 38 kDa (Fig. S1) were pooled, dialyzed four times against 10 mM sodium phosphate buffer at pH 7.3 and concentrated by ultrafiltration.

Purified SLAC-DC-His and SLAC-His solutions were incubated with $CuSO_4$ corresponding to five times the concentration of the enzyme at 4°C for several hours. SLAC-DC-His aggregates were collected by centrifugation (Fig. S2a). SLAC-His was dialyzed against 50 mM ammonium bicarbonate buffer and lyophilized for long-term storage. Protein concentrations were determined by Bradford assay with bovine serum albumin standards for both SLAC-His and SLAC-DC-His and by absorbance at 590 nm with the extinction coefficient 4400 M^{-1} cm^{-1} for SLAC-His after the addition of $CuSO_4$ (Machczynski et al., 2004).

Kinetic characterization

The activity of SLAC-DC-His aggregates for 2,6-Dimethylphenol (DMP) was verified visually after the addition of 10 mM DMP, and SLAC-DC-His aggregates formed in the presence of single-walled carbon nanotubes were also active (Fig. S2d). 20 μL samples containing 1.8 mg of SLAC-His and pre-formed SLAC-DC-His aggregates were incubated with an equal volume of SWNT ink for 1 hour at room temperature. Samples were also prepared in which SLAC-DC-His aggregates were formed after incubating SLAC-DC-His with the SWNT ink. Samples were then diluted 100x and assayed in 10 mM DMP. Measurements were performed in triplicate on a Spectramax M2 plate reader (Molecular Devices, Sunnyvale, CA), and reactions were monitored at 468 nm for the formation of the dimeric product 3,3',5,5'-tetramethoxydiphenylquinone (Fig. S3) with the extinction coefficient 14,800 M^{-1} cm^{-1}. Activities were normalized by their activity without SWNTs (Table S2).

Dilute protein solutions were prepared to determine kinetic activities by adding $CuSO_4$ to 200 nM SLAC-DC-His. Protein solutions were incubated for several hours at 4°C with $CuSO_4$ corresponding to 5 times the concentration of enzyme. SLAC-DC-His activity was determined using concentrations ranging from 0 – 100 mM DMP in air-saturated 10 mM sodium phosphate buffer pH 7.3 with a final enzyme concentration of 20 nM. Measurements were performed in triplicate, and reactions were monitored at 468 nm. All data were fit to the Michaelis-Menten equation using SigmaPlot nonlinear regression software (Fig. S4).

Transmission Electron Microscopy (TEM)

SLAC-DC-His aggregates with a final concentration of 0.7 mg/mL following a 10x dilution were negatively stained with 1% uranyl acetate in water on a carbon coated 400 mesh Cu/Rh grids that had been glow discharged for 1 minute before use. Samples were imaged on a Philips CM12 Tungsten Emission TEM (FEI, Eindhoven, Netherlands) at 120 kV with a Gatan 4 k x 2.67 k digital camera (Gatan Inc., Pleasanton, CA).

Aggregate Size Analysis

Samples of SLAC-DC-His with a concentration of 7 mg/mL were incubated for 20 minutes on ice, room temperature, and 50°C. $CuSO_4$ was then added and samples were incubated for 1 hour under the same conditions. Samples were diluted 100x then imaged using an Olympus CKX41 microscope with a Canon EOS 60D camera. At least 6 images per sample were analyzed with ImageJ to determine the area of 800 aggregates (Fig. S5)

Thermostability measurements

Samples containing 200 nM of SLAC-DC-His aggregates or SLAC-His in 10 mM sodium phosphate buffer, pH 7.3, were incubated at 25°C, 70°C, and 98°C for 30 minutes Samples were then cooled on ice for 10 minutes. Three samples at each temperature were assayed for residual activity in 10 mM DMP as described above. Average residual activities were normalized with respect to the residual activities at 25°C.

Rotating Disk Electrode (RDE) measurements

Three different configurations for SLAC-DC-His immobilization and incorporation into the SWNTs matrix were utilized: i) SLAC-DC-His aggregates were adsorbed on a surface modified with SWNTs; ii) pre-formed SLAC-DC-His aggregates were combined with SWNTs; iii) SWNTs were incorporated with SLAC-DC-His during aggregation. For the first configuration, 30 μL of the SWNT ink was deposited on the surface of RDE and dried under nitrogen. Then 20 μL (0.9 mg) of SLAC-DC-His aggregates in 0.1 M phosphate buffer (pH 7.5) was dropped on the SWNTs surface and dried at

ambient conditions. For the second configuration, 20 μL of the SWNT ink was deposited on the surface of RDE and dried under nitrogen. 1.8 mg of SLAC-DC-His after their aggregation were dissolved in 20 μL of 0.1 M phosphate buffer (pH 7.5), mixed with 20 μL of the SWNT ink and left at ambient temperature for 1 hour. Then 20 μL of this enzyme-nanotubes assembly was dropped on the surface of the already placed SWNTs and dried under ambient conditions. For the final configuration in which the SWNTs were incorporated with SLAC-DC-His prior to their aggregation, 20 μL of the SWNT ink was deposited on the surface of the RDE and dried under nitrogen. 1.8 mg of SLAC-DC-His before aggregate formation was initiated in 20 μL of 0.1 M phosphate buffer (pH 7.5) was mixed with 20 μL of the SWNT ink and left at ambient temperature for 1 hour. $CuSO_4$ was added to the mixture and incubated so SLAC-DC-His aggregates can form in the presence of the SWNTs. Then 20 μL of this enzyme-nanotubes assembly was dropped on the surface of the already placed SWNTs and dried under ambient conditions.

An enzyme-free control electrode was prepared by depositing 20 μL of the SWNT ink on the surface of the RDE and then dried under nitrogen. A second control electrode with the control enzyme SLAC-His was also prepared. 20 μL of the SWNT ink was deposited on the surface of RDE and dried under nitrogen. 1.8 mg of SLAC-His were dissolved in 20 μL of 0.1 M phosphate buffer (pH 7.5), mixed with 20 μL of the SWNT ink and left at ambient temperature for 1 hour. Then 20 μL of this enzyme-nanotubes assembly was dropped on the surface of the already placed SWNTs and dried under ambient conditions. A third control electrode with denatured SLAC-His was also prepared. SLAC-His was incubated at 98°C for 1 hour in the presence of 8 M urea, dialyzed three times against 0.1 M phosphate buffer (pH 7.5) and checked for loss of activity for DMP. 20 μL containing 1.8 mg of denatured SLAC-His was mixed with 20 μL of the SWNT ink and left at ambient temperature for 1 hour. Then 20 μL of this enzyme-nanotubes assembly was dropped on the surface of the already placed SWNTs and dried under ambient conditions. Each of the studied electrodes had 0.9 mg of enzyme per electrode.

All electrochemical measurements were performed in a three-electrode configuration with the cathode connected as working electrode, saturated Ag/AgCl and Pt-wire as reference and counter electrodes, respectively. 0.1 M phosphate buffer (pH 7.5) was used as electrolyte. For the RDE measurements, Pine Research Instrumentation rotator (Grove City, PA) coupled with a VersaSTAT 3 potentiostat (Princeton Applied Research, Oak Ridge, TN). Linear sweep voltammetry from 0.8 to -0.60 V vs. Ag/AgCl with 10 mV/s and different rotating rates was carried out in oxygen depleted, oxygen saturated and an electrolyte with dissolved oxygen (Fig. S6). Reverse scans were initially performed, but it was found that they did not provide any additional information and were excluded from subsequent measurements for simplicity. RDE measurements of SWNT-modified electrodes without enzyme were performed as a control (Fig. S7). The oxygen concentration during the RDE measurements was monitored using DO probe. Three independent identical electrodes for each cathode type were prepared and tested for reproducibility.

Temperature-controlled RDE measurements

The modified RDE electrodes were introduced into electrochemical cell, and the temperature of the electrolyte was kept for 30 minutes at 25, 50 and 70°C, respectively, using a water jacket. Linear sweep voltammetry from 0.8 to -0.60 V vs. Ag/AgCl with 10 mV/s and 1600 rpm was carried out in oxygen saturated electrolyte (Fig. S8). Current densities at -50 mV with the SWNT control current density subtracted were used as comparison. Three independent identical cathodes were tested at each temperature for reproducibility.

Gas-diffusion cathodes

SLAC-DC-His was incorporated in the design of gas-diffusion cathodes. The cathodes were composed of plastic case, carbon black Vulcan X72, modified with 35% of polytetrafluoroethylene referred in this study as XC35 for the development of the gas-diffusion layer (GDL) and 100 mg of XC35 covered by a mixture of 50 mg XC35, 50 mg SWNTs and SLAC-DC-His aggregates formed in presence of SWNTs as it was described before, or SLAC-His explored as a catalytic layer (CL) (Fig. S9). The CL was

pressed at 500 psi for 5 min and circular discs with 0.15 cm diameter were cut for the cathode assembly. The final loading of SLAC-DC-His or SLAC-His per electrode was 9.2 μg of enzyme. Ni wire going from the catalytic layer through the GDL was placed for electrical contact. This cathode design allows manufacturing of multiple electrodes from a single XC35-carbon black-SLAC pressed tablet and thus increases the reproducibility of the preparation procedure. Pure oxygen was blown from the outer side of the GDL while potentiostatic polarization curves were obtained using a Gamry 600 potentiostat (Warminster, PA). Three independent identical electrodes for each cathode type were prepared and tested for reproducibility.

Results and Discussion

The guiding principle in the assembly design process is to introduce a single new dimeric interface between SLAC protein molecules, which, in combination with the threefold symmetry of SLAC, will drive self-assembly of a material. Following the geometric constraints presented by Padilla et al. (Padilla et al., 2001), the SLAC enzyme can be assembled into a P 41 3 2 crystal architecture via a dimer interface between two trimers by constraining the angle between the respective dimer and trimer symmetry axes to 35.3 degrees. The design principle is illustrated in Fig. 1a. Beginning with two SLAC molecules in a two-fold symmetric arrangement, additional copies of SLAC bound with identical binding modes to the first pair, gradually build a coherent symmetric assembly.

Disulfide bonds were chosen to drive interface formation. This both simplifies the interface design problem and yields a very stable connection between subunits in an oxidizing environment. The symmetric angular constraint described above, along with the requirement that the trimers must be in contact with one another in order to form an interface, drastically limits the number of possible interfaces that can form the desired structure (King et al., 2012).

This limited set of compatible binding modes was searched exhaustively with Rosetta for shape complementarity and cross-interface positions capable of accommodating a disulfide bond (King et al., 2014). One such disulfide-compatible geometry was found to be very similar to a crystal contact in the SLAC crystal structure (PDB id 3CG8), making it likely to be physically reasonable, and was selected as the design of choice. The chosen disulfide-mediated interface is shown in Fig. 1b. The new mutations (Gly70 and Ala189 mutated to Cys) were made to SLAC-His using site-directed mutagenesis and the resultant protein with a C-terminal polyhistidine tag was named SLAC-DC-His.

Kinetic parameters for SLAC-DC-His and SLAC-His were determined in dilute solution with the substrate 2,6-dimethoxyphenol (DMP) (Table 1 and Fig. S4). We have previously observed that the addition of an N-terminal polypeptide fusion can dramatically decrease the turnover number (kcat) compared to the wild-type while fusions to the C-terminus had a far less impact (Szilvay et al., 2011; Wheeldon and Gallaway, 2008). The double cysteine mutations in SLAC-DC-His did not significantly affect the turnover number compared to SLAC-His. However, the Michaelis constant K_M is larger for SLAC-DC-His, resulting in a decreased catalytic efficiency (k_{cat}/K_M).

Purified SLAC-DC-His was studied for aggregate formation. Blue aggregates were seen to form in an oxidative environment when $CuSO_4$ was incubated with samples containing SLAC-DC-His (Fig. S2a). TEM images of the aggregates showed assemblies with regions of 3-fold symmetry consistent with the computational design (Fig. 1c). Protein aggregates were not seen to form when SLAC-His was exposed to the same conditions. SLAC-DC-His aggregates also formed in the presence of SWNTs after the addition of $CuSO_4$ (Fig. S2b). Aggregates formed with and without SWNTs were found to be active with DMP (Fig. S2d), and SWNTs were not found to significantly affect enzyme activity for DMP (Table S2). SLAC-DC-His aggregates were dissolved upon addition of the reducing agent dithiothreitol (DTT) (Fig. S2c). Aggregates

exhibited a large variation of sizes (Fig. S5). The aggregates did not appear to dissolve after storing them in buffer over a period of months.

In order to explore electrochemical function of the SLAC aggregates, rotating disk electrode (RDE) measurements were used to study the rate of oxygen reduction, which eliminates diffusional limitations and allows the study of oxygen reduction reaction activity in kinetically limited conditions. Three main electrochemical parameters were used for comparison: generated current density, onset and half-wave potentials (Bard and Faulkner, 2001). The onset potential provides information for the thermodynamic aspect of the reaction, and a higher onset potential is an indication for decreased overpotential of the reaction or decreased activation energy. The generated current is descriptive for the kinetics of the oxygen reduction reaction, and higher current densities are indicative of improved reaction kinetics. The half-wave potential gives information for both the thermodynamics and kinetics of the process. It is the potential of a voltammetric curve at the point where the difference between the faradaic current and the non-faradaic current is equal to one-half of the limiting current.

To provide increased surface area and a better contact between the electrode and the enzyme aggregates, SWNTs were explored. This technique was applied to study the electrochemical activity of SLAC-DC-His aggregates when combined with SWNTs in three configurations: i) SLAC-DC-His aggregates were adsorbed on a surface modified with SWNTs; ii) pre-formed SLAC-DC-His aggregates were combined with SWNTs; iii) SWNTs were incorporated with SLAC-DC-His during aggregation. For each configuration, current production from the oxygen reduction reaction was observed, and the current was linearly dependent on the oxygen concentration (Fig. 2). Redox peaks observed with oxygen-depleted electrolyte were also observed without the enzyme catalyst and are likely due to impurities in the SWNTs (Fig. S7). The enzymatic aggregates were stably absorbed on the rotating disk electrodes, and we did not visually observe loss of the deposited ink even at rotation rates of 1600 rpm.

Comparing the electrochemical response of the SLAC-DC-His/SWNT composites, a sequential increase in the oxygen reduction reaction current densities can be seen, demonstrating the importance of enzyme-nanomaterial interfacial interactions (Fig. 3). The increase in current density observed when SLAC-DC-His aggregates are combined with SWNTs before being deposited onto the electrode is likely due to increased contacts between the enzymes and the SWNTs. Contact between the SWNTs and enzyme active sites is further increased in the case where SWNTs were introduced into a solution of purified SLAC-DC-His before aggregation was initiated. This enabled self-assembly to entrap SWNTs within the aggregates. This approach dramatically increased current densities during oxygen reduction. The generated current at -0.15 V and 19.8 ± 4.2 mg/mL oxygen content was 3.5 times higher than the preformed SLAC-DC-His aggregates mixed with SWNTs and 4.2 times higher than the physically adsorbed aggregates.

The nonspecific incorporation of the SWNTs into SLAC-DC-His assemblies not only leads to enhanced current generation but also a significant positive shift in the onset potential, from 0.075 V vs. Ag/AgCl for SLAC-His to 0.220 V vs. Ag/AgCl for SLAC-DC-His, and half-wave potential of approximately 100 mV, from - 0.168 V vs. Ag/AgCl for SLAC-His to -0.070 V vs. Ag/AgCl for SLAC-DC-His (Fig. 3). These indicate a decrease of the reaction overpotential and improvement in kinetics are most likely due to the decreased tunneling distance and the orientation of the enzyme active site (Ramírez et al., 2008). Based on the Butler-Volmer equation, a decrease in reaction overpotential by 100 mV leads to a 90 times increase in reaction kinetics and generated current.

SLAC-His and SLAC-DC-His aggregates were incubated at elevated temperatures and assayed in solution for DMP oxidation activity at room temperature in order to compare the resistance to irreversible thermal denaturation (Table 2). After incubation at 70°C, the residual activities of both samples decreased, with SLAC-His exhibiting a larger decrease in activity.

This difference was more pronounced for the samples incubated at 98°C. The activity of the SLAC-His samples was reduced by 99% while the SLAC-DC-His samples retained 43% of the original activity.

Electrochemical activities were also measured at elevated temperatures for RDE electrodes (Table 3, Fig. S8). At 50°C, there is no statistically significant difference in the retained activities of the SLAC-His/SWNTs and SLAC-DC-His/SWNTs composites. At 70°C, the SLAC-DC-His/SWNTs composite demonstrated higher electrochemical activity than the SLAC-His/SWNTs composite, retaining 47% activity. These results indicate that SLAC-DC-His aggregates are more resistant to thermal denaturation than SLAC-His. Although it is unlikely that these electrodes would be operated at these higher temperatures, the increased resistance to thermal denaturation is likely due to the prevention of irreversible unfolding or the facilitated refolding enabled by the engineered disulfide bonds, and this would likely lead to increased operational lifetimes at ambient temperatures.

Gas diffusion cathodes are advantageous due to the higher oxygen concentration available for reduction at the cathode compared to in solution. Therefore, the SLAC-DC-His assembly with incorporated SWNTs was integrated into the design of an air-breathing cathode and compared to a SLAC-His air- breathing cathode via steady state polarization curves (Fig. 4). The current density at 0.0 V vs. Ag/AgCl recorded with the gas-diffusion SLAC-DC-His cathode was 1.1 mA/cm^2, which was significantly higher than the SLAC-His cathode. The SLAC-DC gas-diffusion cathode outperformed the SLAC-His cathode design throughout the potential region tested.

This result can be compared to previous reports in the literature. A laccase-based gas-diffusion cathode with an identical design to the one used in this study generated 0.70 mA/cm^2 using air as the source of oxygen (Gupta et al., 2011a). The interactions between the enzyme and the carbon black material relied on physical adsorption of the enzyme and direct electron

transfer from the electrode to SLAC. To improve the direct electron transfer rate in the current design, we incorporated SWNTs along with the protein engineering approach and thus achieved 1.5 times higher current densities in comparison to the same miniature GDE exploring laccase as catalyst. Bilirubin oxidase (BOx) gas-diffusion cathode where BOx was physically adsorbed on the electrode surface demonstrated 0.35-0.50 mA/cm^2 (Gupta et al., 2011b). When an orienting agent (syringaldazine) and a tethering agent (1-pyrenebutanoic acid, succinimidyl ester) were used for more efficient enzyme orientation, improved electron transfer and stability, the current densities of a BOx-GDE reached 0.70 mA/cm^2 (Ulyanova et al., 2014). Using more complex tethering agent 4,4′-[(8,16-dihydro-8,16-dioxodibenzo[a,j]perylene-2,10-diyl)dioxy] dibutyric acid di(N-succinimidyl ester (DDPSE) and no orienting agent in the construction of laccase cathode demonstrated ~0.44 mA/cm^2 (Lau et al., 2012).

Conclusion

In conclusion, we have used computational protein design to create a SLAC double mutant that can self-assemble into active enzymatic crystalline-like assemblies. The enzyme aggregates were easily immobilized by physical adsorption, enabling high enzyme loadings. Additionally, the nonspecific incorporation of SWNTs into the aggregates led to improved kinetics from increased enzyme-SWNT contacts. The self-assembly increased resistance to thermal denaturation. A current density of 1.1 mA/cm^2 at 0 V vs. Ag/AgCl was achieved in an air-breathing cathode system. This designed self-assembly approach could be employed to create new biomaterials from other enzymes for use in biofuel cells as well as many other biocatalysis applications.

Acknowledgments

We thank S. Namazi, Dr. G. Szilvay and Dr. E. Campbell for their technical contributions to the project. This work was funded by the Air Force Office of Scientific Research.

References

Addo PK, Arechederra RL, Minteer SD. 2010. Evaluating Enzyme Cascades for Methanol/Air Biofuel Cells Based on NAD+-Dependent Enzymes. Ed. Evgeny Katz, Plamen Atanassov. *Electroanalysis* **22**:807–812.

Babanova S, Artyushkova K, Ulyanova Y, Singhal S, Atanassov P. 2014. Design of experiments and principal component analysis as approaches for enhancing performance of gas-diffusional air-breathing bilirubin oxidase cathode. *Journal of Power Sources* **245**:389–397.

Bard AJ, Faulkner LR. 2001. Electrochemical Methods: Fundamentals and Applications 2nd ed. New York: John Wiley and Sons.

Barton SC, Gallaway J, Atanassov P. 2004. Enzymatic biofuel cells for implantable and microscale devices. *Chem. Rev.* **104**: 4867-4886.

Cooney MJ, Svoboda V, Lau C, Martin G. 2008. Enzyme catalysed biofuel cells. *Energy & Environmental Science* **1**:320–337.

Davila D, Esquivel JP, Vigues N, Sanchez O, Garrido L, Tomas N, Sabate N, del Campo FJ, Munoz FJ, Mas J. 2008. Development and optimization of microbial fuel cells. *Journal of New Materials for Electrochemical Systems* **11**:99–103.

Gallaway J, Wheeldon I, Rincon R, Atanassov P, Banta S, Barton SC. 2008. Oxygen-reducing enzyme cathodes produced from SLAC, a small laccase from Streptomyces coelicolor. *Biosensors and Bioelectronics* **23**:1229–1235.

Glykys DJ, Szilvay GR, Tortosa P, Suárez Diez M, Jaramillo A, Banta S. 2011. Pushing the limits of automatic computational protein design: design, expression, and characterization of a large

synthetic protein based on a fungal laccase scaffold. *Syst Synth Biol* **5**:45–58.

Gupta G, Lau C, Branch B, Rajendran V, Ivnitski D, Atanassov P. 2011a. Direct bio-electrocatalysis by multi-copper oxidases: Gas-diffusion laccase-catalyzed cathodes for biofuel cells. *Electrochimica Acta* **56**:10767–10771.

Gupta G, Lau C, Rajendran V, Colon F, Branch B, Ivnitski D, Atanassov P. 2011b. Direct electron transfer catalyzed by bilirubin oxidase for air breathing gas-diffusion electrodes. *Electrochemistry Communications* **13**:247–249.

Holland JT, Lau C, Brozik S, Atanassov P, Banta S. 2011. Engineering of Glucose Oxidase for Direct Electron Transfer via Site-Specific Gold Nanoparticle Conjugation. *J. Am. Chem. Soc.* **133**:19262–19265.

Jiang L, Althoff EA, Clemente FR, Doyle L, Rothlisberger D, Zanghellini A, Gallaher JL, Betker JL, Tanaka F, Barbas CF, Hilvert D, Houk KN, Stoddard BL, Baker D. 2008. De Novo Computational Design of Retro-Aldol Enzymes. *Science* **319**:1387–1391.

Kim J, Jia H, Wang P. 2006. Challenges in biocatalysis for enzyme-based biofuel cells. *Biotechnology Advances* **24**:296–308.

King NP, Sheffler W, Sawaya MR, Vollmar BS, Sumida JP, Andre I, Gonen T, Yeates TO, Baker D. 2012. Computational Design of Self-Assembling Protein Nanomaterials with Atomic Level Accuracy. *Science* **336**:1171–1174.

King NP, Bale JB, Sheffler W, McNamara DE, Gonen S, Gonen T, Yeates TO, Baker D. 2014. Accurate design of co-assembling multi-component protein nanomaterials. *Nature* **510**:103–108.

Korkegian A, Black ME, Baker D, Stoddard BL. 2005. Computational Thermostabilization of an Enzyme. *Science* **308**:857–860.

Lau C, Adkins ER, Ramasamy RP, Luckarift HR, Johnson GR, Atanassov P. 2012. Design of Carbon Nanotube-Based Gas-Diffusion Cathode for O2 Reduction by Multicopper Oxidases. *Advanced Energy Materials* **2**:162–168.

Lim J, Cirigliano N, Wang J, Dunn B. 2007. Direct electron transfer in nanostructured sol-gel electrodes containing bilirubin oxidase. *Phys. Chem. Chem. Phys.* **9**:1809–1814.

Logan BE, Hamelers B, Rozendal R, Schröder U, Keller J, Freguia S, Aelterman P, Verstraete W, Rabaey K. 2006. Microbial fuel cells: methodology and technology. *Environ. Sci. Technol.* **40**:5181–5192.

Luckarift HR, Atanassov PB, Johnson GR. 2014. Enzymatic fuel cells: From fundamentals to applications. New York: John Wiley and Sons.

Machczynski MC, Vijgenboom E, Samyn B, Canters GW. 2004. Characterization of SLAC: A small laccase from Streptomyces coelicolorwith unprecedented activity. *Protein Sci.* **13**:2388–2397.

Minteer SD, Liaw BY, Cooney MJ. 2007. Enzyme-based biofuel cells. *Current Opinion in Biotechnology* **18**:228–234.

Padilla JE, Colovos C, Yeates TO. 2001. Nanohedra: Using symmetry to design self assembling protein cages, layers, crystals, and filaments. *Proceedings of the National Academy of Sciences* **98**:2217–2221.

Ramírez P, Mano N, Andreu R, Ruzgas T, Heller A, Gorton L, Shleev S. 2008. Direct electron transfer from graphite and functionalized gold electrodes to T1 and T2/T3 copper centers of bilirubin oxidase. *Biochimica et Biophysica Acta (BBA) - Bioenergetics* **1777**:1364–1369.

Szilvay GR, Brocato S, Ivnitski D, Li C, Iglesia PDL, Lau C, Chi E, Werner-Washburne M, Banta S, Atanassov P. 2011. Engineering of a redox protein for DNA-directed assembly. *Chem. Commun.* **47**:7464–7466.

Tsujimura S, Kamitaka Y, Kano K. 2007. Diffusion-Controlled Oxygen Reduction on Multi-Copper Oxidase-Adsorbed Carbon Aerogel Electrodes without Mediator. *Fuel Cells* **7**:463–469.

Ulyanova Y, Babanova S, Pinchon E, Matanovic I, Singhal S, Atanassov P. 2014. Effect of enzymatic orientation through the use of syringaldazine molecules on multiple multi-copper oxidase enzymes. *Phys. Chem. Chem. Phys.* **16**:13367–13375.

Usui K, Maki T, Ito F, Suenaga A, Kidoaki S, Itoh M, Taiji M, Matsuda T, Hayashizaki Y, Suzuki H. 2009. Nanoscale elongating control of the self-assembled protein filament with the cysteine-introduced building blocks. *Protein Sci.* **18**:960–969.

Wheeldon IR, Gallaway JW, Barton SC, Banta S. 2008. Bioelectrocatalytic hydrogels from electron-conducting metallopolypeptides coassembled with bifunctional enzymatic building blocks. *Proc. Natl. Sci.* **105**: 15275-15280.

Wong TS, Schwaneberg U. 2003. Protein engineering in bioelectrocatalysis. *Current Opinion in Biotechnology* **14**:590–596.

Tables

Table 1. Kinetic parameters of SLAC-DC-His and SLAC-His for DMP oxidation. Measurements were performed in triplicate, and represented with their mean and standard deviation from the mean.

	K_M [mM]	k_{cat} [min^{-1}]	k_{cat}/K_M [$mM^{-1}min^{-1}$]
SLAC-DC-His	13 ± 2[a]	110 ± 10	8.2 ± 1.6[a]
SLAC-His	4.7 ± 0.4	120 ± 10	25 ± 2

[a] $p < 0.01$, where statistical significance of SLAC-DC-His parameters compared to the control SLAC-His were calculated by unpaired two-sample t-test

Table 2. Residual specific activities of SLAC-His and SLAC-DC-His for DMP oxidation measured at 25°C after 30 minute incubation at elevated temperatures. Measurements were performed in triplicate, normalized by the activity at 25°C and represented with their mean and standard deviation from the mean.

	25°C	70°C	98°C
SLAC-DC-His	1.0 ± 0.1	0.50 ± 0.08[a]	0.43 ± 0.08[a]
SLAC-His	1.0 ± 0.1	0.31 ± 0.05[a]	0.011 ± 0.004[a]

[a] $p < 0.01$, where statistical significance compared to measurements at 25°C calculated by unpaired two-sample t-test

Table 3. Retained electrochemical activity of SLAC-His/SWNTs and SLAC-DC-His/SWNTs composites where SWNTs were incorporated prior to aggregation. Measurements were performed in triplicate, normalized by the activity at 25°C and represented with their mean and standard deviation from the mean.

	25°C	50°C	70°C
SLAC-DC-His	1.0 ± 0.1	0.77 ± 0.10[b]	0.47 ± 0.03[a]
SLAC-His	1.0 ± 0.1	0.81 ± 0.02[b]	0.05 ± 0.04[a]

[a] $p < 0.01$, where statistical significance compared to measurements at 25°C calculated by unpaired two-sample t-test

[b] $p < 0.05$, where statistical significance compared to measurements at 25°C calculated by unpaired two-sample t-test

List of Figures

Figure 1. Design of the SLAC-DC-His assembly: A) Illustration of one-interface design principle, wherein a single new interface gives rise to self-assembly. Shown is the stepwise application of the dimer interface to terminal SLAC-DC-His trimers, adding new trimers to the assembly until a fully connected crystalline architecture is attained. B) Detail of the designed dimer interface between SLAC-DC-His trimers, showing the two disulfide linkages which form the interface as green, blue and yellow spheres. The active site copper atoms are also shown as gold spheres. C)TEM image of SLAC-DC-His aggregates.

Figure 2. RDE measurements of A) SLAC-DC-His aggregates adsorbed on SWNTs B) pre-formed SLAC-DC-His aggregates mixed with SWNT inks, and C) SWNTs incorporated into SLAC-DC-His aggregates. Experiments were performed in an oxygen depleted electrolyte (solid lines), oxygen saturated electrolyte (dash dotted lines) and an electrolyte exposed to air (dashed lines) (10 mV/s, 1600 rpm). Insets (reproduced for clarity in Fig. S10) show the dependence of the current density at -0.15 V vs. Ag/AgCl on the oxygen concentration in the electrolyte with SLAC-DC-His aggregates (triangles), SLAC-His (squares) and SWNTs only (diamonds). Three independent identical electrodes for each cathode type were prepared and tested for reproducibility. The results are represented with the mean from the three measurements and the standard deviation from the mean.

Figure 3. RDE measurements of SWNTs only (solid black line), SLAC-His mixed with SWNTs (gray line), denatured SLAC-His mixed with SWNTs (gray dashed line), SLAC-DC-His aggregates adsorbed on SWNTs (dashed line) pre-formed SLAC-DC-His aggregates mixed with SWNT ink (dash dotted line) and SLAC-DC-His with incorporated SWNTs before aggregation (dotted line) in electrolyte exposed to ambient air (10 mV/s and 1600 rpm).

Figure 4. Potentiostatic polarization curves for SLAC-DC-His aggregates (circles), SLAC-His (triangles) and neat SWNTs (squares) when incorporated into the design of a gas-diffusion cathode with 9.2 μg of enzyme deposited on each cathode. Three independent identical electrodes for each cathode type were prepared and tested for reproducibility. The results in the figure are represented with the mean and the standard deviation from the mean.

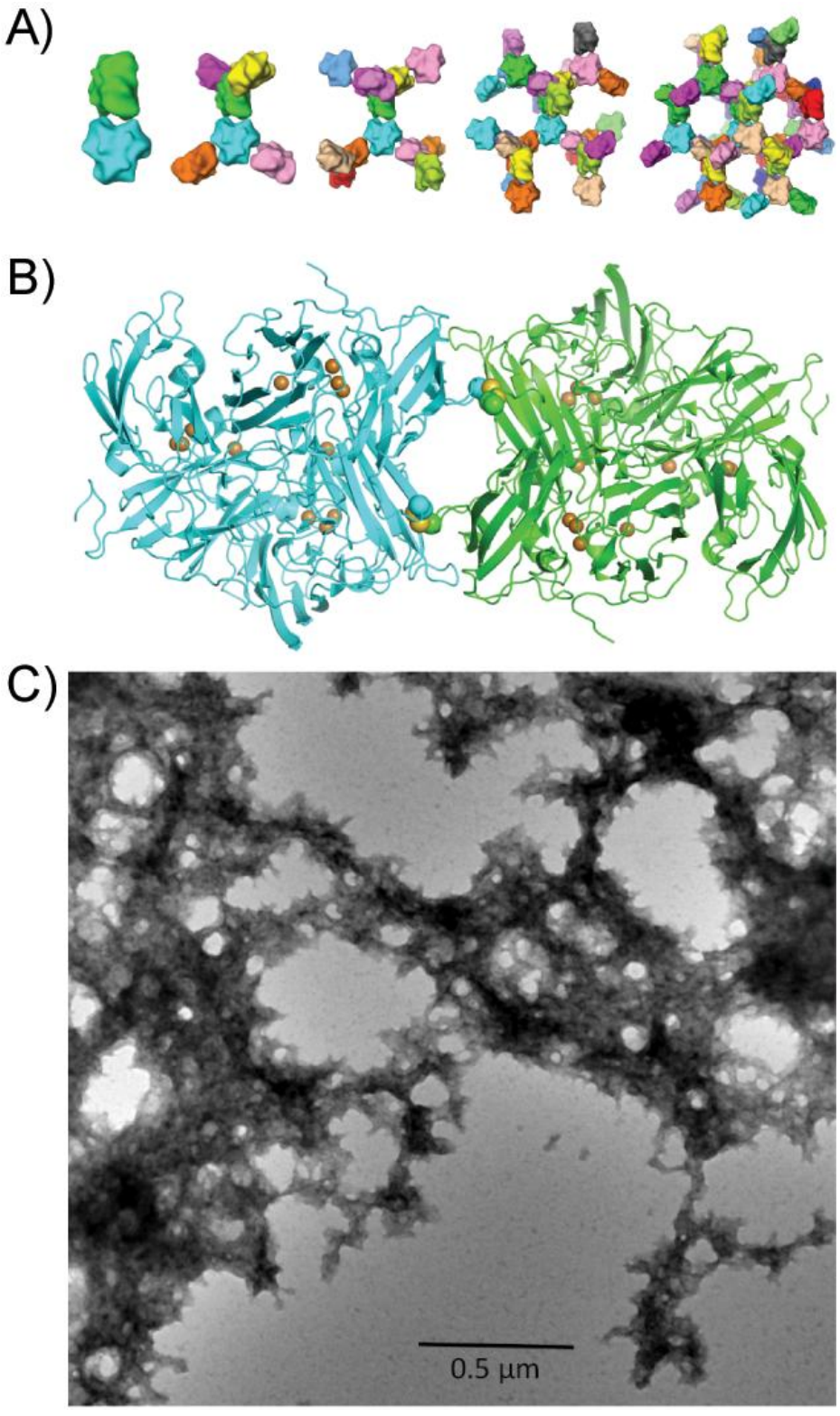

Figure 1

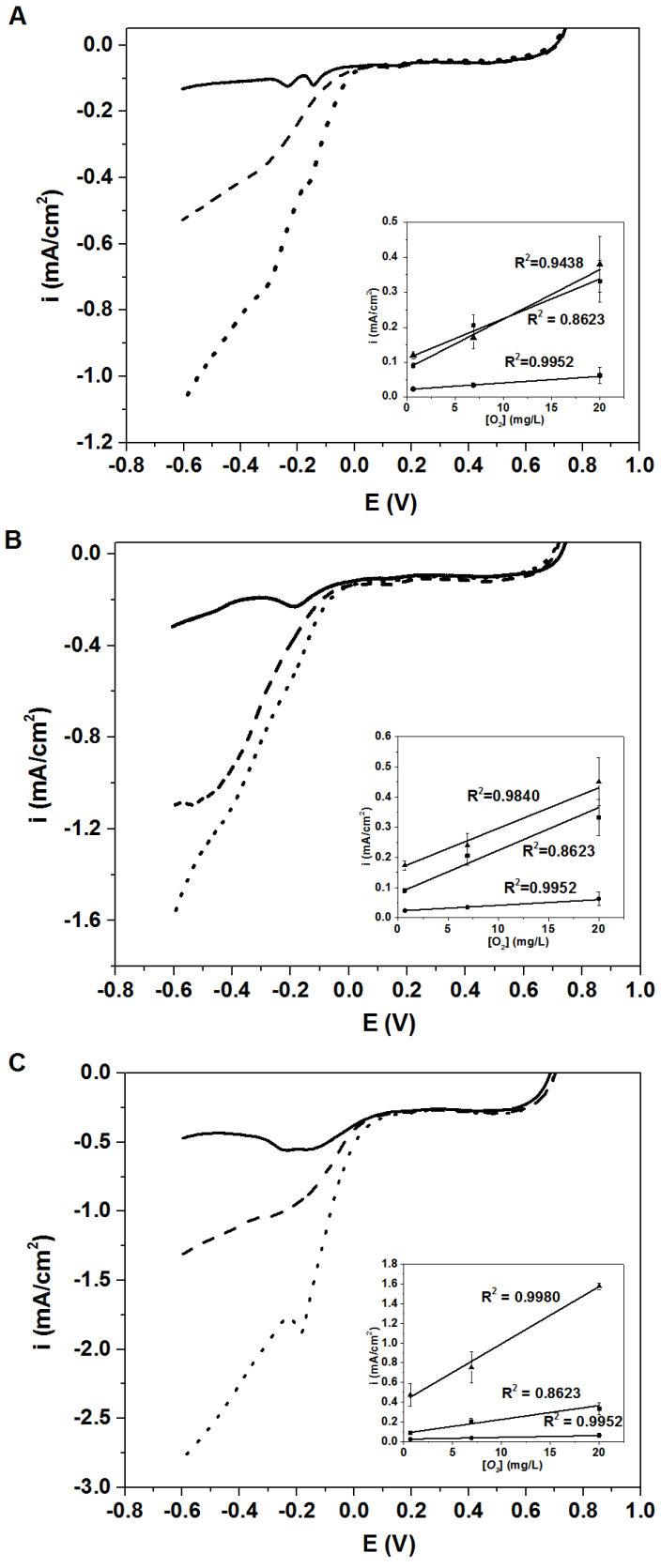

Figure 2

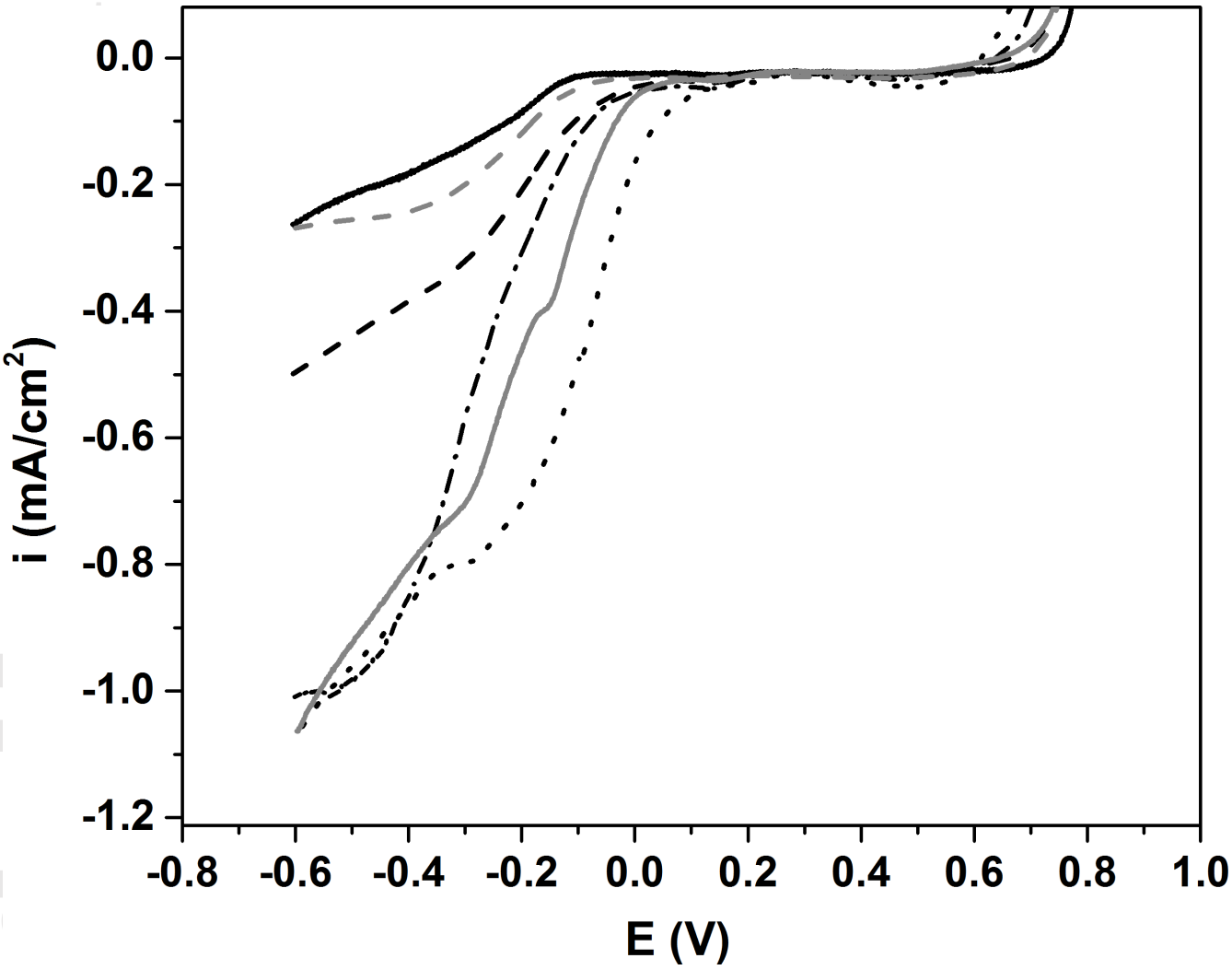

Figure 3

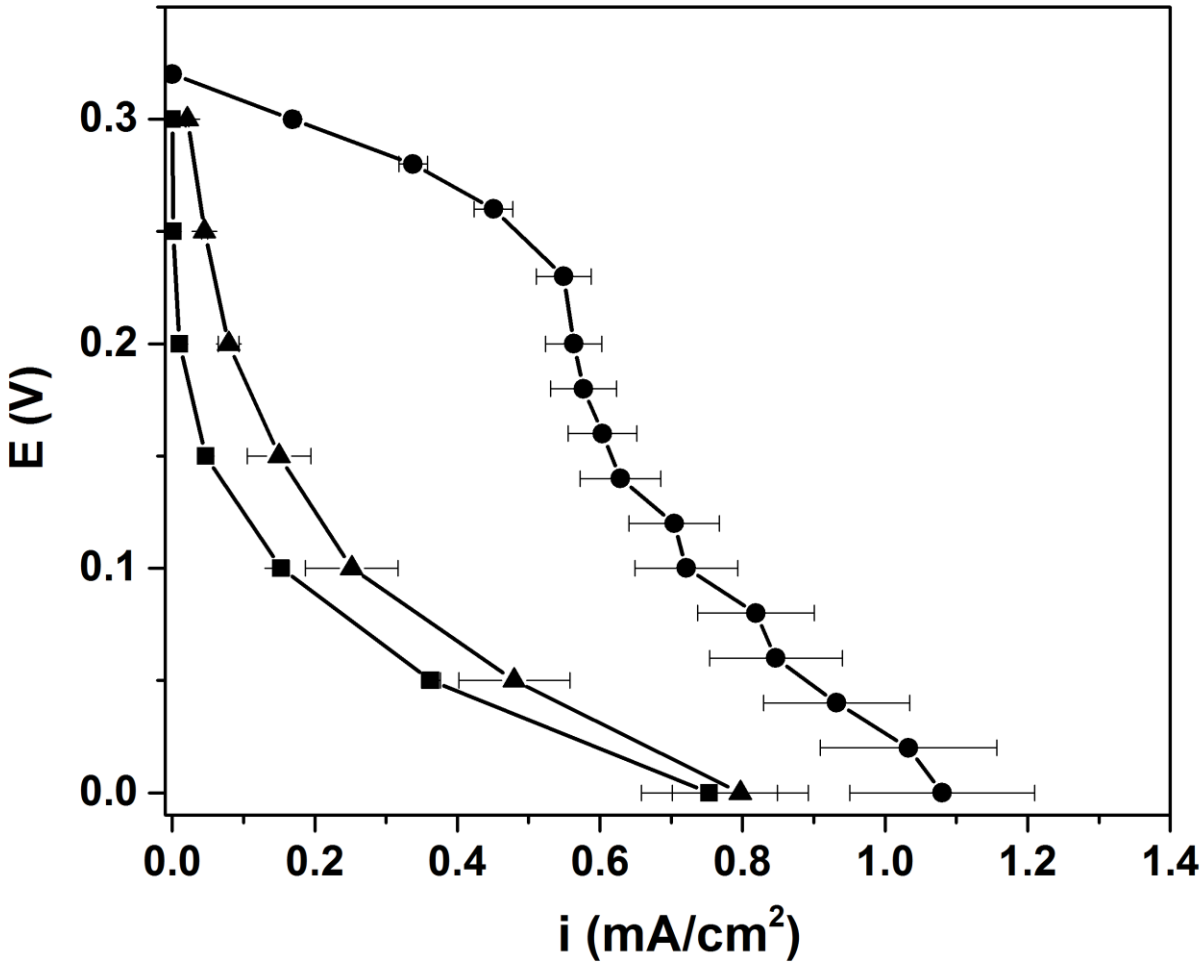

Figure 4